Microwave Radiometric Measurements of Sea Surface Temperature from the Seasat Satellite: First Results

Abstract. *Initial results from the Seasat scanning multichannel microwave radiometer indicate that the sea surface temperature can be measured with a root-mean-square sensitivity of 1.2°C or better. The first microwave map of sea surface temperature for the entire Pacific has been produced.*

Global sea surface temperature (SST) monitoring is of interest because of the influence of SST on weather and climate; SST data are also of interest to oceanographers. Infrared radiometric techniques have been used to monitor SST from satellites, but these techniques are limited by atmospheric water, mainly clouds (*1*). Microwave radiometry is also sensitive to SST; it is less limited than infrared radiometry by atmospheric water but more limited by surface roughness. The scanning multichannel microwave radiometer (SMMR) on the Seasat satellite (also on Nimbus-7, both launched in 1978) was the first satellite-borne microwave experiment whose major goal was SST measurement. This report presents initial results from the Seasat SMMR experiment. General references on microwave remote sensing are given in (*2*). Microwave techniques have been used to measure atmospheric temperature profiles, water vapor, liquid water, polar ice boundaries, ice type, and other geophysical parameters from satellites (*3*). Special issues of *Science* (29 June 1979) and the *IEEE Journal of Oceanic Engineering* (April 1980) have been devoted to the Seasat mission and sensors.

The SMMR, designed and fabricated by the Jet Propulsion Laboratory, measures microwave radiation from the earth's surface and atmosphere at wavelengths of 0.8, 1.4, 1.7, 2.8, and 4.5 cm and at two linear polarizations for each wavelength. Each of these ten channels is sensitive in a different manner to various geophysical parameters. [Wilheit (*4*) has reviewed the principles.] In general, the shorter wavelength SMMR channels are more sensitive to atmospheric effects and the longer wavelength channels are more sensitive to surface effects. The polarization of the radiation is determined by the specular surface contribution to the total radiance. A rougher surface, and atmospheric effects, depolarize the radiation. The SMMR field of view is produced by a 79-cm offset-parabolic reflector which is sinusoidally scanned over a 50° swath angle with a period of 4.1 seconds. The scan is conical with a nominal 42° nadir angle, which provides an earth-incidence angle of approximately 49° (varying by approximately 1° as a result of changing satellite orientation). The full width (at half-power points) of the antenna beam at the earth's surface varies from 28 km by 18 km at a wavelength of 0.8 cm to 136 km by 89 km at a wavelength of 4.5 cm. The SMMR design and instrument performance are described in (*5*). The Seasat orbit was nearly circular with an altitude of 795 km and an inclination of 108°. The 14 daily revolutions provided 95 percent global coverage by the SMMR below a latitude of 75° every 36 hours.

The algorithm used here for retrieving geophysical parameters from the SMMR is described in detail by Hofer and Njoku (*6*). It is a piecewise-linear relationship between appropriate functions of the SMMR measurements and the desired parameters. We determined the coefficients describing this relationship from numerical simulations of the experiment, using an ensemble of atmospheric and surface conditions. The root-mean-square SMMR accuracies predicted from these simulations are 0.8°C for SST, 1.5 m/sec for surface wind speed (which is sensed by its effect on surface roughness), 0.2 g/cm^2 for vertical-column water vapor, and 4.4 mg/cm^2 for vertical-column liquid water.

The geophysical retrieval algorithm was applied after the SMMR radiometric data were calibrated. The calibration consisted of the on-board radiometric instrument calibration as described by Swanson and Riley (*7*) with corrections determined by 117 comparisons of SMMR measured radiances and calculated radiances. These comparisons were done in the northeast Pacific (30°N to 55°N, 195°E to 235°E) where conventional measurements of geophysical parameters were available. Data from four Seasat orbital revolutions between 13 and 25 September 1978 were used. The conventional data included the September 1978 National Marine Fisheries Service (NMFS) SST map (*8*), surface wind fields produced by Cardone (*9*) for the time and location of Seasat overpasses, and measurements from National Oceanic and Atmospheric Administration buoys 46005 and 46006. A latitude-dependent climatological water vapor value (*10*) was used. Only cloud-free and rain-free situations (identified from SMMR) were used. The resulting corrections applied (as simply an additive constant) to the measured radiances amounted to between −5° and +10°C "brightness temperature" (equivalent radiance blackbody temperature) for the various SMMR channels. Corrections of approximately this size were expected in order to achieve agreement between the calculated and measured radiances. Such agreement must be achieved so that the retrieval coefficients derived from numerical simulations can be appropriately applied to the SMMR data. Whether these corrections are required because of residual errors in on-broad instrument calibration, because of inaccuracies in the theoretical expressions used for calculations, because of inadequate geophysical data, or because of a combination of these causes has not been determined.

To estimate the accuracy of SMMR

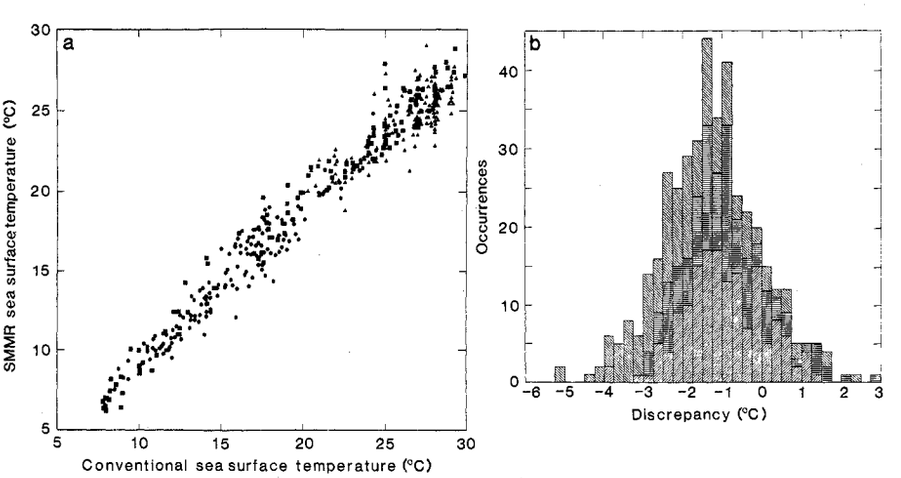

Fig. 1. Comparative plot of 418 Seasat SMMR and conventional SST measurements: (a) scatterplot; (b) histogram of discrepancies. Three conventional data sets, whose locations are indicated in Fig. 2a, were used for these comparisons: (●, ///) XBT; (■, ≡) NMFS map for the north Pacific area; and (▲, \\\) NMFS map for the tropical Pacific area.

0036-8075/81/0619-1385$00.50/0

Table 1. Results of a comparison of SMMR and conventional measurements of SST in July 1978. The regions are indicated in Fig. 2a.

Conventional data type and region	Comparisons (No.)	Conventional measurements (°C)			Discrepancies (°C)		
		Range	Mean	σ	Range	Mean	σ
XBT	156	7.4 to 26.2	15.2	3.9	−3.8 to 1.4	−1.0	1.0
NMFS map, north Pacific	125	7.8 to 29.9	20.6	6.8	−3.0 to 2.9	−1.0	1.1
NMFS map, tropical Pacific	137	20.3 to 29.3	26.1	2.3	−5.2 to 2.3	−1.9	1.4
All of the above	418	7.8 to 29.9	20.7	6.2	−5.2 to 2.9	−1.3	1.2

SST measurements derived from the algorithms and calibrations described above, we compared SMMR and conventional measurements of the Pacific during July 1978. Corrections obtained from only the September 1978 data set were applied to the July SMMR data, and so we expect no "inbreeding" of the July comparisons and the calibration corrections. The conventional measurements for the comparisons were obtained from expendable bathythermograph (XBT) observations between 14 and 24 July 1978, from the "TRANSPAC ship of opportunity program in the North Pacific" (*11*), and from the July 1978 NMFS SST map digitized to a 5° latitude by 5° longitude grid. The SMMR measurements made between 16 and 23 July 1978 were first used to produce a map. [Because of averaging (*12*), the effective resolution of this map is 149 km by 149 km.] Values from this map were then interpolated to the locations of the conventional measurements for a total of 418 actual comparisons. The SMMR accuracy estimated from these comparisons is an upper limit, since some error is expected in the conventional measurements and some error also arises from the temporal and spatial interpolations required to compare the SMMR and conventional measurements. We estimate that these errors may contribute up to approximately half the total measured root-mean-square discrepancy.

Figure 1a shows the 418 July comparisons between SMMR and conventional SST measurements; Fig. 1b is a histogram of the discrepancies (defined as SMMR measurements minus conventional measurements). The locations of the comparisons are indicated in Fig. 2a, which also gives the NMFS SST map for July 1978. Table 1 gives the range, mean, and standard deviation (σ) of the conventionally measured SST values and of the discrepancies between SMMR and conventional measurements. Improved calibration and retrieval algorithms should remove the mean discrepancy (if there is no mean error in the conventional data). The σ values of the discrepancies for these comparisons appear uncorrelated with the σ values of the conventional measurements. This result suggests that the SMMR measurements are mainly limited by instrumental and geophysical noise. However, the 30 percent larger σ of the discrepancies in the tropics also suggests that some improvements in the retrieval algorithms are possible. Similar comparisons for surface wind speed and vertical water vapor column gave root-mean-square discrepancies of 2 m/sec and 0.4 g/cm^2, respectively (*13*).

Figure 2b shows the SMMR Pacific SST map made from 47 descending Seasat orbital revolutions which occurred between 16 and 23 July 1978. The SMMR measurements of each revolution were interpolated to a 1° latitude by 1° longitude grid. Approximately half the map's grid points contain information from two different revolutions; no grid point contains information from more than four revolutions. We rejected two SMMR measurement points in making this map: one because of radio frequency interference, the other because of data transmission errors. The major features of the SMMR map are in good agreement with the NMFS map (Fig. 2a). There is a strong north-south gradient around 40°N and a plateau in the tropical Pacific. A region of colder water separates this plateau from the Central American coastline.

The warm area in Fig. 2b around 15°N, 235°E is attributable to a rain cell evident in the SMMR retrievals for atmospheric liquid water. The north-south features in the SMMR map around, for example, 25°N, 180°E are thought to be residual instrumental scan-dependent calibration effects. Influences of continental coasts and major island areas, which appear as warm areas, were not filtered out of the

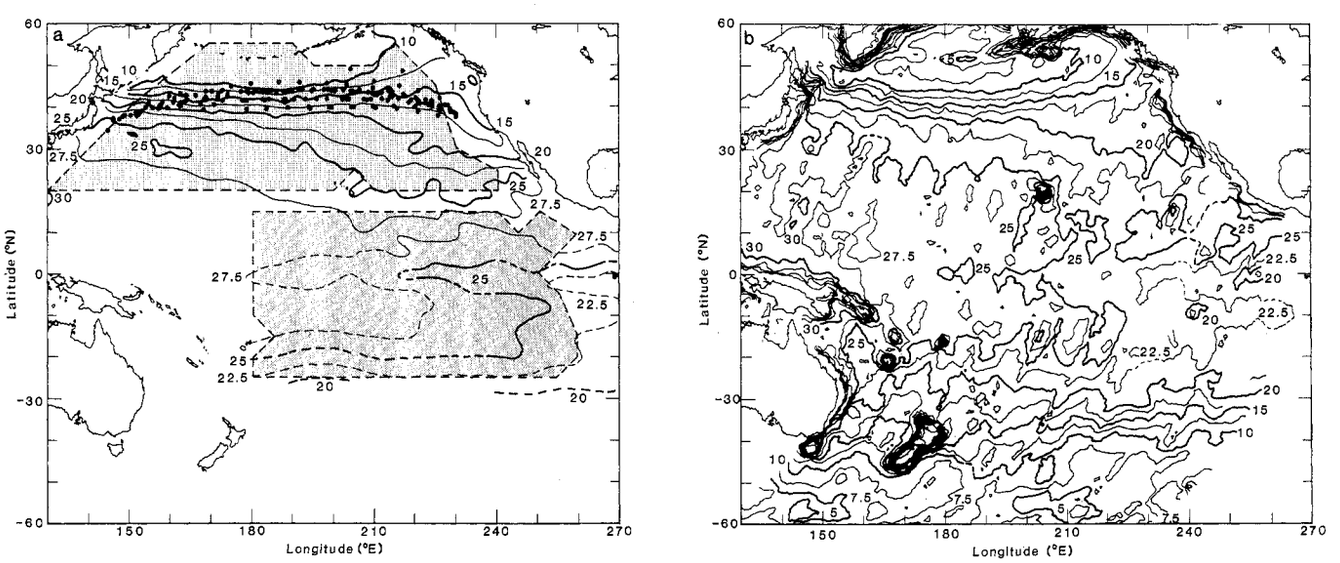

Fig. 2. (a) The NMFS SST map for July 1978 and locations for the comparison data sets. Dashed contours are based on sparse data; circles indicate the locations of XBT measurements. (b) Seasat SMMR SST map for 16 to 23 July 1978. Dashed contours are interpolations for missing data. The map contours in (a) and (b) are 2.5°C.

SMMR data used for this map. This influence occurs out to approximately 1000 km from major land areas. Implementation of a side-lobe correction algorithm (*12*) will reduce this distance to approximately 300 km (two resolution cells) as tests on limited Seasat data sets have indicated.

These results indicate that microwave radiometers orbiting the earth can measure SST with a root-mean-square sensitivity of 1.2°C or better. Better results will probably be possible with improved instrument calibration, sensitivity, and retrieval algorithms.

R. HOFER*
E. G. NJOKU
J. W. WATERS
Earth and Space Sciences Division,
Jet Propulsion Laboratory,
California Institute of Technology,
Pasadena 91109

References and Notes

1. T. P. Barnett, W. C. Patzert, S. C. Webb, B. R. Bean, *Bull. Am. Meteorol. Soc.* **60**, 197 (1979). However, work is under way to reduce these limitations: M. T. Chahine, in *Remote Sensing of Atmospheres and Oceans*, A. Deepak, Ed. (Academic Press, New York, 1980), p. 411; E. P. McClain, in *Oceanography from Space* (proceedings of the COSPAR/SCOR/IUCRM symposium, Venice, Italy, 1980) (Plenum, New York, in press), p. 73; P. Y. Deschamps and T. Phulpin, *Boundary-Layer Meteorol.* **18**, 131 (1980).
2. D. H. Staelin, *Proc. IEEE* **57**, 427 (1969); K. Tomiyasu, *ibid.* **62**, 86 (1974); E. Schanda, in *Ecological Studies*, vol. 18, *Remote Sensing for Environmental Sciences*, E. Schanda, Ed. (Springer, Berlin, 1978), p. 187.
3. D. H. Staelin, A. H. Barrett, J. W. Waters, F. T. Barath, E. J. Johnston, P. W. Rosenkranz, N. E. Gaut, W. B. Lenoir, *Science* **182**, 1339 (1973); D. H. Staelin, P. W. Rosenkranz, F. T. Barath, E. J. Johnston, J. W. Waters, *ibid.* **197**, 991 (1977); D. H. Staelin, K. F. Kunzi, R. L. Pettyjohn, R. K. L. Poon, R. W. Wilcox, J. W. Waters, *J. Appl. Meteorol.* **15**, 1204 (1976); T. T. Wilheit, A. T. C. Chang, M. S. V. Rao, E. B. Rodgers, J. S. Theon, *ibid.* **16**, 551 (1977); J. W. Waters, K. F. Kunzi, R. L. Pettyjohn, R. K. L. Poon, D. H. Staelin, *J. Atmos. Sci.* **32**, 1953 (1975); A. T. C. Chang and T. T. Wilheit, *Radio Sci.* **14**, 793 (1979); T. T. Wilheit, *Boundary-Layer Meteorol.* **13**, 277 (1978); ———, A. T. C. Chang, A. S. Milman, *ibid.* **18**, 65 (1980); W. J. Campbell, R. O. Ramseier, H. J. Zwally, P. Gloersen, *ibid.*, p. 99; K. F. Kunzi, A. D. Fisher, D. H. Staelin, J. W. Waters, *J. Geophys. Res.* **81**, 4965 (1976).
4. T. T. Wilheit, *IEEE Trans. Geosci. Electron.* **GE-17**, 244 (1979).
5. E. G. Njoku, J. M. Stacey, F. T. Barath, *IEEE J. Oceanic Eng.* **OE-5**, 100 (1980).
6. R. Hofer and E. G. Njoku, *IEEE Trans. Geosci. Remote Sensing*, in press. Other algorithms have also been developed; for example: P. W. Rosenkranz, *Radio Sci.* **13**, 1003 (1978); T. T. Wilheit and A. T. C. Chang, *ibid.* **15**, 525 (1980); F. J. Wentz, in *Seasat Gulf of Alaska Workshop Report 1* (internal publication 622–101, Jet Propulsion Laboratory, Pasadena, Calif., 1979), pp. 8–19.
7. P. N. Swanson and A. L. Riley, *IEEE J. Oceanic Eng.* **OE-5**, 116 (1980).
8. J. A. Renner, Ed., *Fishing Information*, produced monthly by the National Oceanic and Atmospheric Administration National Marine Fisheries Service, Southwest Fisheries Center, La Jolla, Calif.
9. V. J. Cardone, in *Seasat Gulf of Alaska Workshop II Report* (internal publication 622-107, Jet Propulsion Laboratory, Pasadena, Calif., 1979), pp. 2–6.
10. J. P. Peixoto and A. R. Crisi, *Hemispheric Humidity Conditions During the IGY* (Department of Meteorology, Massachusetts Institute of Technology, Cambridge, 1965), p. 17.
11. W. B. White and R. L. Bernstein, *J. Phys. Oceanogr.* **9**, 592 (1979).
12. E. G. Njoku, E. J. Christensen, R. E. Cofield, *IEEE J. Oceanic Eng.* **OE-5**, 125 (1980).
13. R. Hofer and E. G. Njoku, in preparation.
14. We thank R. Bernstein of the Scripps Institution of Oceanography for providing the XBT comparison data, J. Kitzis and S. Kitzis for major programming assistance, and the Seasat project personnel for providing the SMMR data. R. Bernstein, M. Chahine, and H. Press made useful comments on the manuscript. R. H. thanks the National Research Council for providing his resident research associate position during this research. The research described in this report was supported in part by the National Academy of Sciences and was carried out at the Jet Propulsion Laboratory, California Institute of Technology, sponsored by the Oceanic Process Branch and the Climate Program Office, Office of Space and Terrestrial Applications, under NASA contract NAS 7-100.
* Present address: CIBA-GEIGY AG, Basel, Switzerland.

24 December 1980; revised 20 March 1981

Hydrovolcanic Explosions: The Systematics of Water-Pyroclast Equilibration

Abstract. *The initial contact of external water with erupting magma and the mass ratio of water to magma govern the development of hydrovolcanic phenomena. The phase relations of water within the runout system and the separation of vapor or liquid from the pyroclasts explain gradational transitions between some pyroclastic flows, base surges, mud hurricanes, mudflows, and sheetfloods.*

Hydrovolcanism refers to volcanic phenomena produced by the interaction of magma or magmatic heat with an external source of water, such as a surface body or an aquifer. There is a complete spectrum of activity, from hydromagmatic to purely magmatic. Most active volcanoes exhibit at least limited periods of hydrovolcanic activity, and it is the dominant type of activity for some volcanoes. Shallow subaqueous eruptions commonly produce hydrovolcanic explosions with ash showers and base-surge clouds, as at Surtsey (1964–1965), Taal (1965), and Capelinhos (1957). Less widely recognized is the subsurface involvement of external water in the explosive eruptions of stratovolcanoes such as Vesuvius (*1*).

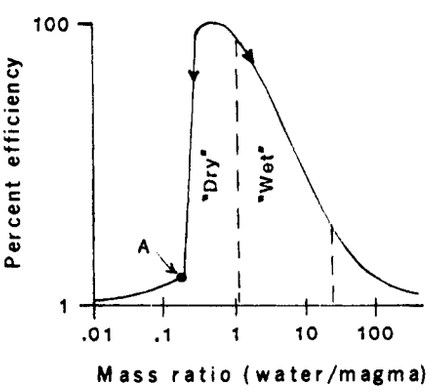

Fig. 1. The conversion efficiency of thermal energy to mechanical energy as a function of the water/magma ratio for the thermite and water system (*4*). The thermal energy per unit mass of thermite is approximately three times that of basalt. Hence the ratio scale must be multiplied by an appropriate factor (3 or 4) to model volcanic systems. With increasing water/magma ratio, the onset of superheating and explosive fragmentation occurs at point *A*.

The 1980 activity of Mount St. Helens has focused attention on the destruction consequent on hydrovolcanic phenomena. This can include debris flows, pyroclastic flows, base surges, mud hurricanes, mudflows, and flash floods (*2*). Even basaltic shield volcanoes exhibit rare hydrovolcanic phases, such as the 1790 and 1924 base-surge eruptions of Kilauea (*3*). This report, which incorporates new data obtained in the field and experimentally (*4*), presents the systematics of water-pyroclast (*5*) interactions as a foundation for a quantitative model of hydrovolcanic activity.

Hydrovolcanic explosions (*6*) produce phenomena that are governed by the initial mixing of magma with water from an external source and the subsequent separation of the entrained water (vapor or liquid) and pyroclasts during eruption and emplacement. The important factors that control the expansion, collapse, and lateral displacement of the system include the mass ratio of water to pyroclasts, the physical state of the water (supercritical fluid, superheated steam, multiphase fluid, or liquid), and the density of the mixture of fluid and particulates.

The initial contact of water and magma, in which thermal energy of the magma is transferred into mechanical energy of the fluid-particulate mixture, determines the subsequent development of hydrovolcanic phenomena. We have conducted a series of experiments to test the effect of the water/magma mass ratio on the efficiency of energy conversions. Data on vapor explosions (*7, 8*) permitted the design of a series of scale-model experiments [involving a large chamber containing mixtures of thermite and water (*4*)] which were used to make first-

0036-8075/81/0619-1387$00.50/0